Temporal Range Registration for Unmanned Ground and Aerial Vehicles★

R. MADHAVAN*, T. HONG and E. MESSINA
Intelligent Systems Division, National Institute of Standards and Technology, Gaithersburg, MD 20899-8230, USA; e-mail: raj.madhavan@ieee.org, {tsai.hong, elena.messina}@nist.gov

Abstract. An iterative temporal registration algorithm is presented in this article for registering 3D range images obtained from unmanned ground and aerial vehicles traversing unstructured environments. We are primarily motivated by the development of 3D registration algorithms to overcome both the unavailability and unreliability of Global Positioning System (GPS) within required accuracy bounds for Unmanned Ground Vehicle (UGV) navigation. After suitable modifications to the well-known Iterative Closest Point (ICP) algorithm, the modified algorithm is shown to be robust to outliers and false matches during the registration of successive range images obtained from a scanning LADAR rangefinder on the UGV. Towards registering LADAR images from the UGV with those from an Unmanned Aerial Vehicle (UAV) that flies over the terrain being traversed, we then propose a hybrid registration approach. In this approach to air to ground registration to estimate and update the position of the UGV, we register range data from two LADARs by combining a feature-based method with the aforementioned modified ICP algorithm. Registration of range data guarantees an estimate of the vehicle's position even when only one of the vehicles has GPS information. Temporal range registration enables position information to be continually maintained even when both vehicles can no longer maintain GPS contact. We present results of the registration algorithm in rugged terrain and urban environments using real field data acquired from two different LADARs on the UGV.

Key words: iterative registration, position estimation, unmanned ground and aerial vehicles, LADAR.

1. Introduction

The National Institute of Standards and Technology (NIST) is developing archi-
tectures and algorithms for unmanned vehicles with funding from the Army Re-
search Laboratory (ARL) and the Defense Advanced Research Projects Agency
(DARPA). The NIST Highly Mobile Multipurpose Wheeled Vehicle (HMMWV)

★ Commercial equipment and materials are identified in this article in order to adequately
specify certain procedures. Such identification does not imply recommendation or endorsement by
the National Institute of Standards and Technology, nor does it imply that the materials or
equipment identified are necessarily the best available for the purpose.

* Corresponding author. Tel. no: (301) 975-2865; Fax: (301) 990-9688.

and an eXperimental Unmanned Vehicle (XUV) developed under the Army's Demo III program [31] serve as test beds for this research. These vehicles are commanded by the hierarchical, distributed, hybrid 4D/RCS (Real-time Control System) architecture [1, 2].

The 4D/RCS architecture developed for Demo III specifies the simultaneous representation of information about entities and events in a hierarchical distributed knowledge database wherein information is presented in a form that is ideally suited for path planning and task decomposition. Maps are populated both with knowledge from a priori sources such as digital terrain databases, and with knowledge from sensors. The range and resolution of maps at different levels are specified to correspond to the range and resolution of planning algorithms. This limits the amount of computational power required to maintain maps and symbolic data structures with a latency that is acceptable for planning and reactive processes at each level.

The position estimation for the above Unmanned Ground Vehicles (UGVs) relies on fusing Global Positioning System (GPS) reported estimates with other on-board navigation sensors. The required accuracy of the GPS estimates cannot be guaranteed for the entirety of a particular mission as the direct line of sight to the satellites cannot be maintained at all times. GPS can be lost due to multipathing effects and terrain conditions, especially for on-road driving tasks. Sufficiently accurate vehicle positions are necessary to derive correct locations of sensed data towards accurate representations of the world and for correctly executing planned trajectories and missions. In order to compensate for such unavailability and unreliability of GPS, another form of secondary position estimation becomes inevitable.

The following reasons also warrant the need to develop robust 3D data registration algorithms:

- Within RCS, the use of *a priori* maps would enhance the scope of the world model. These maps may take a variety of forms including survey and aerial maps and may provide significant information about existing topology and structures. In order to take advantage of this knowledge, research is needed to register these *a priori* maps with the sensor-centric maps [15]. Additionally, for incorporating a priori knowledge into the world model, some form of weighting is required and this depends on how well the *a priori* data and the sensed information are registered.
- There is also the need to generate higher resolution *a priori* terrain maps as the current survey maps are too coarse for off-road autonomous driving and also for maintaining up-to-date representations of the world even if the maps are of higher resolution.
- Another potential application for registering LADAR data is the computation of *ground truth* as such registration is not dependent on time-based drift (unlike inertial navigation systems), vehicle maneuvers and terrain of travel.

Such ground truth is necessary for evaluating performance of navigation algorithms and systems.

Active range sensing has become an integral part of any unmanned vehicle navigation system due its ability to produce unambiguous, direct, robust, and precise images consisting of range pixels, for example, using LAser Detection And Ranging (LADAR) imagery. This is in direct contrast to passive sensing where the inference of range largely remains computationally intensive and not robust enough for use in natural outdoor environments. Depending on the speed of the vehicle, operating environment, and data rate, such range images acquired from a moving platform need to be registered to make efficient use of information contained in them for various navigation tasks within the 4D/RCS architecture.

One of the following two approaches is commonly employed for matching range images to *a priori* maps [13]:

- *Feature-based Matching*: In this approach, two sets of features, $\mathcal{F}_i^1$ and $\mathcal{F}_j^2$, are extracted from two sets to be matched and then correspondences between features, $\mathcal{F}_{ik}^1$ and $\mathcal{F}_{jk}^2$, $k \in i, j$, that are globally consistent, are found. The displacement between the two sets can then be computed to deduce the sensor pose.
- *Point Matching*: This approach directly works on two sets of data points, $\mathcal{P}^1$ and $\mathcal{P}^2$, by minimizing a cost function of the form $\mathbf{F}(\mathbf{T}(\mathcal{P}^2), \mathcal{P}^1)$, where $\mathbf{T}(\mathcal{P}^2)$ is the second set of points subjected to a transformation $\mathbf{T}$. Any sensible cost is acceptable as long as its minimum corresponds to a *best* estimate of $\mathbf{T}$ in some sense. Usually, the minimization leads to an iterative gradient-like algorithm.

Lines and edges are two of the most widely used feature primitives. Matching between sensor observations and modeled features in a map have been considered as a search in an *Interpretation Tree* [10]. Drumheller extracts lines from sonar data and matches them against a room model to enable robot localization [8]. The complexity of the search problem is minimized by applying local constraints (distances, angles and normal directions) to the set of possible pairings between observed and modeled features. The Hough transform is a shape detection technique which can be used to isolate features of a particular shape within an image or Time-of-Flight (TOF) sensor data. Schiele and Crowley extract line segments using the Hough transform from an occupancy grid and update the position of the robot using a Kalman filter [28]. Other researchers [9, 19] have combined odometric data and laser measurements using an extended Kalman filter where the range weighted Hough transform is employed to extract lines from laser data. The resulting peaks are used as feature coordinates. Even though the Hough transform provides good results in indoor cluttered environ-

ments, it is restricted to operating in rectangular-shaped scenarios where no more than two predominant walls are present.

Kanade et al. [18] compared elevation maps obtained from 3D range images to determine vehicle location. A similar point matching approach has also been adopted by Shaffer [29]. Cox [6] proposes a point matching method for an indoor robot named Blanche where scan-points from an optical rangefinder are matched to an *a priori* map composed of straight line segments. Blanche's position estimation system utilizes a robust matching algorithm which estimates the precision of the corresponding match/correction that is then optimally combined with odometric position to provide an improved estimate of robot position. Hoffman et al. employ a point matching algorithm for obtaining the inter-frame rotation and translation in a vision-based rover application [14]. Lu [20] finds corresponding points between two successive scans to compute the relative rotation and translation. An Iterative Dual Correspondence (IDC) algorithm is formulated based on closest point and matching range rules. Olson [26, 27] constructs a three-dimensional occupancy map of the terrain using stereo vision and iconically matches with a similar map to obtain the relative position between the maps enabling a mobile robot to perform self-localization.

The major drawback of the above approaches is that their use is limited to structured office or factory environments rather than unstructured natural environments. Straightforward correlation-based schemes (for e.g., see [35]), in general, are unable to handle outliers. As cross-correlation calculates the similarity, the two scans must be similar and thus this method cannot accommodate occlusions. This is easy to understand since if areas visible in one scan are not visible in another due to occlusion, then correlation of these scans may produce arbitrarily bad pose estimates. Also correlation usually places a high burden on computation especially when the scans are at different orientations.

In this article, we present algorithms for registering 3D range images to overcome both the unavailability and unreliability of GPS within required accuracy bounds for UGV navigation.★ At the core of the registration process is a modified version of the well-known Iterative Closest Point (ICP) algorithm. These modifications render robustness to outliers, occlusions and false matches/ spurious points. We then propose extensions to the ICP algorithm that make it possible to register range images obtained from a UGV to range images obtained from an Unmanned Aerial Vehicle (UAV). Registration of range data guarantees an estimate of the vehicle's position even when only one of the vehicles has GPS information. Temporal range registration enables position information to be continually maintained even when both vehicles can no longer maintain GPS

★ It is important to note that the focus of the present work is primarily on position estimation using registration of range images and not (the related area of) Simultaneous Localization And Mapping (SLAM).

contact. We present results of the registration algorithm using real field data acquired from two different LADARs on the UGV [22].

The article is organized as follows: Section 2 details the ICP algorithm with suitable modifications for robustness. Section 3 presents the results of the proposed algorithm when applied for registering consecutive range images obtained from two LADARs mounted on a moving UGV. Section 4 extends the modified ICP algorithm for air to ground registration by a hybrid feature-based registration approach and elaborates the results of the hybrid approach when employed for registering aerial and ground range images. Finally, Section 5 provides conclusions and describes further research work.

2. Iterative Temporal Range Registration Algorithm

We term the process of *registration* as follows: *Given two sets of 3D range images (model set*: **M** *and data set*: **D**): *Find a 3D transformation* (*rotation and translation*) *which when applied to* **D** *minimizes a distance measure between the two point sets*.

The goal can be stated more formally as:

$$min_{(\mathbf{R},\mathbf{T})} \sum_i \|\mathbf{M}_i - (\mathbf{R}\mathbf{D}_i + \mathbf{T})\|^2 \tag{1}$$

where **R** is a 3×3 rotation matrix, **T** is a 3×1 translation vector and the subscript i refers to the corresponding points of the sets **M** and **D**.

We adapt the ICP algorithm for registering 3D LADAR range images. The algorithm as we have applied to register range images with suitable modifications is given in the next section.

2.1. ITERATIVE CLOSEST POINT ALGORITHM

The ICP algorithm [4] can be summarized as follows: Given an initial motion transformation between the two 3D point sets, a set of correspondences are developed between data points in one set and the next. For each point in the first data set, find the point in the second that is closest to it under the current transformation. It should be noted that correspondences between the two points sets is initially unknown and that point correspondences provided by sets of closest points is a reasonable approximation to the true point correspondence. From the set of correspondences, an incremental motion can be computed facilitating further alignment of the data points in one set to the other. This find correspondence/compute motion process is iterated until a predetermined threshold termination condition.

In its simplest form, the ICP algorithm can be described by the following   189
steps: 190

1. For each point in data set **D**, compute its closest point in data set **M**. In this   191
   article, this is accomplished via 3D nearest point search from the set   192
   comprising $N_{\mathbf{D}}$ data and $N_{\mathbf{M}}$ model points.   193
2. Compute the incremental transformation (**R**, **T**) using Singular Value   194
   Decomposition (SVD) using correspondences obtained in step **1**.   195
3. Apply the incremental transformation from step **2.** to **D**.   196
4. If relative changes in **R** and **T** are less than a threshold, terminate. Else go to   197
   step **1**.   198

To deal with spurious points/false matches and to account for occlusions and   199
outliers, we modify and weight the least-squares objective function in Equation   200
(1) such that [36]:   201

$$min_{(\mathbf{R},\mathbf{T})} \sum_i w_i \|\mathbf{M}_i - (\mathbf{R}\mathbf{D}_i + \mathbf{T})\|^2 \tag{2}$$

If the Euclidean distance between a point x_i in one set and its closest point y_i 202
in the other, denoted by $d_i \triangleq d(x_i, y_i)$, is bigger than the maximum tolerable   205
distance threshold $\mathcal{D}_{max}$, then w_i is set to zero in Equation (2). This means that   206
an x_i cannot be paired with a y_i since the distance between reasonable pairs   207
cannot be very big. The value of $\mathcal{D}_{max}$ is set adaptively in a robust manner by   208
analyzing distance statistics.   209
Let $\{x_i, y_i, d_i\}$ be the set of original points, the set of closest points and their   210
distances, respectively. The mean and standard deviation of the distances are   211
computed as: 212

$$\mu = \frac{1}{N} \sum_{i=1}^{N} d_i; \ \sigma = \sqrt{\frac{1}{N} \sum_{i=1}^{N} (d_i - \mu)^2}$$

where N is the total number of pairs.   213
The pseudo-code for the adaptive thresholding of the distance $\mathcal{D}_{max}$ is given   215
below: 216

```
    if μ < D
D^{itn}_{max} = μ + 3σ;
  else if μ < 3D
D^{itn}_{max} = μ + 2σ;
  else if μ < 6D
  D^{itn}_{max} = μ + σ;
  else D^{itn}_{max} = ε;
```

where *itn* denotes the iteration number and $\mathcal{D}$ is a function of the resolution of   217
the range data.   219

During implementation, $\mathcal{D}$ was selected based on the following two   220
observations: 221

1) If $\mathcal{D}$ is too small, then several iterations are required for the algorithm to   222
   converge and several good matches will be discarded, and   223
2) If $\mathcal{D}$ is too big, then the algorithm may not converge at all since many   224
   spurious matches will be included. The interested reader is referred to [36]   225
   for more details on the effect and selection of $\mathcal{D}$ and ϵ on the convergence of   226
   the algorithm.   227

At the end of this step, two corresponding point sets, $\mathbf{P_M}:\{\mathbf{p}_i\}$ and $\mathbf{P_D}:\{\mathbf{q}_i\}$ are   228
available.   229

The incremental 3D transformation (rotation and translation) of step **2.** is   230
obtained as follows [3]:   231

- Calculate $\mathbf{H} = \sum_{i=1}^{N_D}(\mathbf{p}_i - \mathbf{p}_c)(\mathbf{q}_i - \mathbf{q}_c)^T$; $(\mathbf{p}_c, \mathbf{q}_c)$ are the centroids of the   233
  point sets $(\mathbf{P_M}, \mathbf{P_D})$.   234
- Find the Singular Value Decomposition (SVD) of $\mathbf{H}$ such that $\mathbf{H} = \mathbf{U}\Omega\mathbf{V}^T$ 235
  where $\mathbf{U}$ and $\mathbf{V}$ are unitary matrices whose columns are the singular vectors   236
  and Ω is a diagonal matrix containing the singular values.   237
- The rotation matrix relating the two point sets is given by $\mathbf{R} = \mathbf{V}\mathbf{U}^T$.   238
- The translation between the two point sets is given by $\mathbf{T} = \mathbf{q}_c - \mathbf{R}\mathbf{p}_c$.   239

This process is iterated as stated in step **4.** until the mean Euclidean distance   240
between the corresponding point sets $\mathbf{P_M}$ and $\mathbf{P_D}$ is less than or equal to a   241
predetermined distance or until a given number of iterations is exceeded.   242

3. Temporal Registration of 3D Range Images   243

In this section, we present the results of the modified iterative algorithm on   244
two sets of LADAR data (henceforth referred to as UGVL1 and UGVL2).   245
Utilizing knowledge about the LADAR mount position and calibration factors,   246
the range information provided by the LADARs are transformed to cartesian   247
coordinates.   248

3.1. EXPERIMENTAL SETUP AND RESULTS   249

The eXperimental Unmanned Vehicle (XUV) shown in Figure 1(a) is a   250
hydrostatic diesel, four-wheel-drive, four-wheel-steer vehicle. The military High   251
Mobility Multipurpose Wheeled Vehicle (HMMWV) shown in Figure 1(b) is a   252
one and one quarter ton, diesel-powered four-wheel-drive truck actuated with   253

Figure 1. The Demo III XUV shown in (a) can drive autonomously at speeds of up to 60 km/h on-road, 35 km/h off-road in daylight, and 15 km/h off-road at night or under inclement weather conditions. (b) shows the NIST HMMWV and (c) its sensor suite.

electric motors for steering, braking, throttle, transmission, transfer case, and park rake and sensors to monitor speed, engine RPM and temperature.

Both vehicles utilize the NIST developed RCS architecture using Neutral Message Language (NML) communications for autonomous navigation in unstructured and off-road driving conditions. The sensor suite of the XUV and the HMMWV (shown in Figure 1(b)) consists of a pair of cameras for stereo vision, a Schwartz Electro-Optics LADAR, a stereo pair of Forward Looking Infra-Red (FLIR) cameras, a stereo pair of monochrome cameras, Global Positioning System (GPS), Inertial Navigation System (INS), a force bumper sensor and actuators for steering, braking and transmission. An integrated Kalman filter navigation system fuses observations from odometry, inertial and differential GPS sensors for position estimation.

UGVL1 data was obtained during field trials as the XUV traversed rugged terrain with vegetation. The LADAR was mounted on this UGV on a pan/tilt platform to increase its narrow 20° field of view. The range of the tilt motion is ±30° resulting in an effective field of view of about 90°. UGVL1 provides a range image of 32 lines × 180 pixels where each data point contains the distance

to a target in the operating environment. The angular resolution of this LADAR 271
is $0.658° \times 0.5°$ in the horizontal and vertical directions, respectively. 272

UGVL2 (Riegl LADAR in Figure 1(b)) data was collected from a sensor 273
mounted on the HMMWV as the vehicle traversed urban environments. The 274
effective field of view is $80° \times 330°$ thus providing an almost panoramic view of 275
the environment with an angular resolution of $0.036°$. The scan rate of UGVL2 is 276
$1°/s - 15°/s$ providing 10,000 pts/s with range up to 800 m thus making it much 277
lower than that of UGVL1 but the resulting 3D range image is of a much higher 278
resolution. For more details on the LADARs, see [30]. 279

In the case of UGVL2, the 3D point cloud was acquired from two different 280
view points whereas for UGVL1, the 3D point cloud represents scan points that 281
were acquired between two consecutive vehicle locations. Additionally, for 282
UGVL1, range image **D** was also translated a meter along each of the (x, y, z) 283
axes in addition to the translation and rotation that the image underwent due to 284
the motion of the vehicle. It is important to note here that even though the range 285
image points arrive in the same sequence for both the model and data sets, it is 286
not guaranteed that both sets will have the same number of points as some facets 287
of the LADAR data sets might return empty values. 288

Figures 2(a) and (b) show the results when the modified ICP algorithm is used 289
to register 3D range images obtained from UGVL1 and Figures 3(a) and (b) 290
show that for UGVL2. The number of model (**M**) and data (**D**) points for the two 291
LADARs are {2,857, 2,878} and {125,396, 123,826}, respectively. As can be 292
seen from Figures 2 and 3, the images are well registered. The closest point 293
distance for UGVL1 before and after registration shown in Figure 4 also proves 294
that the images are sufficiently registered. The mean distance (m) after regis- 295
tration for the above three cases are {0.11, 0.84, 0.43}, respectively. 296

Table I summarizes the registration results for two data sets obtained using 297
UGVL1. In data set #2, point sets separated by 20 scans were matched. In data 298
set #4, range image **D** of data set #1 was rotated $10°$ and was also translated 3 m 299
along each of the (x, y, z) axes. Due to the above translation and rotation, it can 300
be seen that both the number of iterations and the mean distance after registration 301
have increased but the range images are still sufficiently registered. Note that 302
such amounts of translation and rotation are highly unlikely to occur between 303
consecutive range images. 304

4. Air to Ground Feature-Based Registration 305

Another way to minimize the dependency on GPS for UGV navigation is to 306
use aerial survey maps constructed using a downward-looking LADAR 307
mounted on an Unmanned Aerial Vehicle (UAV). If the LADAR range images 308
from the UGV can be registered to those from the UAV, then these results can 309
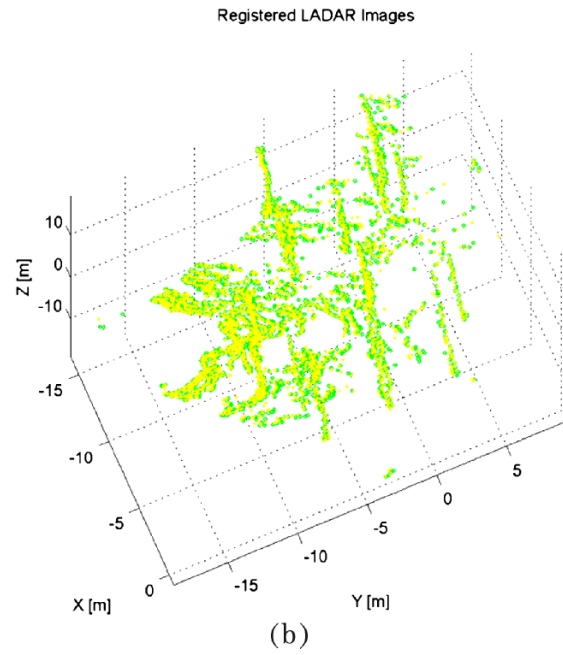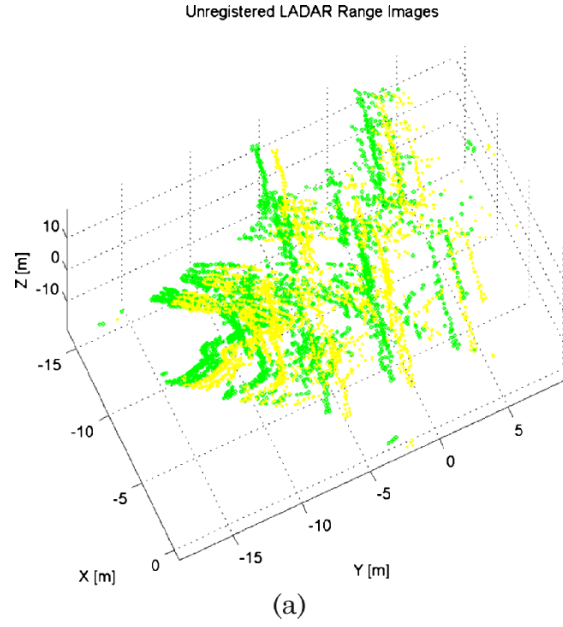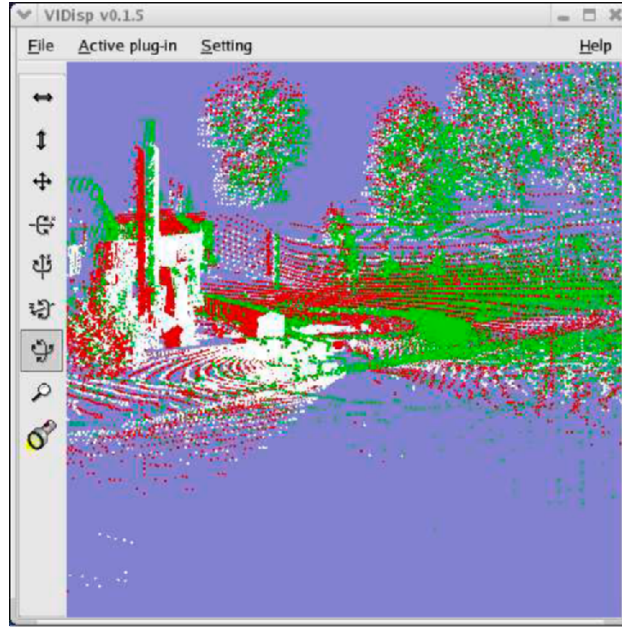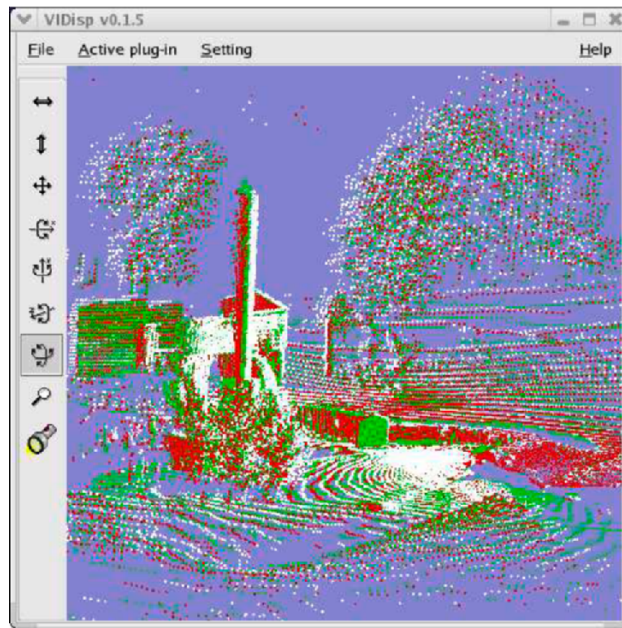serve as secondary position estimates in the event of absence or degradation of 310
GPS.

Figure 2. 3D LADAR range images before and after registration. (a) and (b) show the unregistered and registered UGVL1 range images, respectively. Here, the data range image (**D** denoted by '○' in yellow) was deliberately translated 1 m along the (x, y, z) axes in addition to the inherent translation to demonstrate the robustness of the iterative algorithm.

TEMPORAL RANGE REGISTRATION FOR UNMANNED GROUND AND AERIAL VEHICLES

(a)

(b)

Figure 3. (a) and (b) show the unregistered and registered range images corresponding to two sets of UGVL2 range images. In (a) and (b), the model (**M**) range image is shown in *green*, unregistered and registered data (**D**) range images are shown in *red* and *white*, respectively.
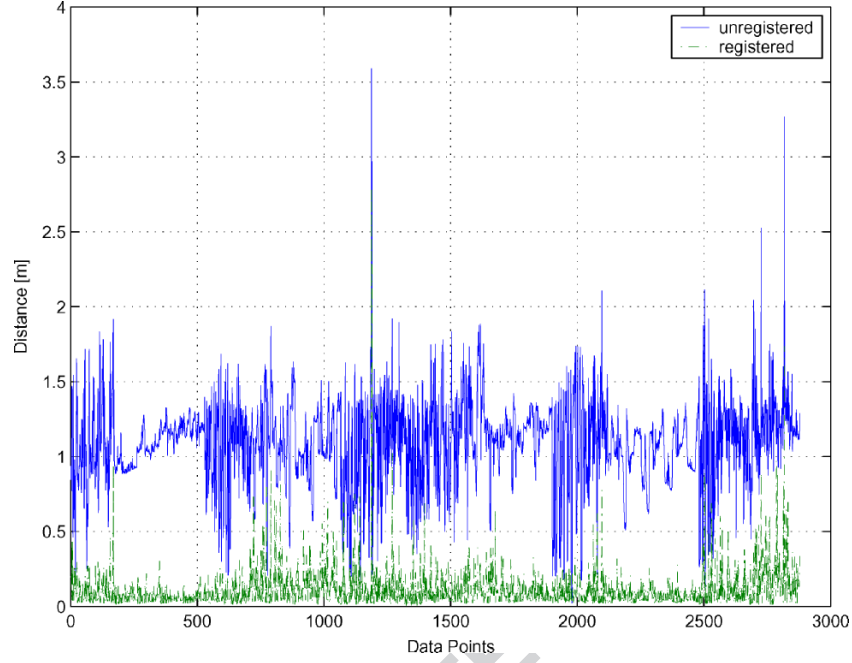
Figure 4. The closest point distance before and after registration of UGVL1 range images.

In this section, we propose a hybrid approach by combining the modified ICP 320
algorithm with a feature-based method for registering two sets of LADAR range 321
images. The proposed approach is conceptually similar to Hebert et al. [12] who 322
employ range imagery to compute vehicle displacement between two viewing 323
positions by using a two-stage technique (feature matching followed by point 324
matching). The advantage of our hybrid approach lies in the fact that the 325
accuracy of the point matching technique is retained while keeping the 326
computational burden under control as the feature-based method provides a 327
good initial estimate for refinement. 328

Table I. Quantitative comparison of performance.

Data set	Description	Mean dist. after registration [cm]	Number of iterations	
				t1.1
				t1.2
#1 **M**:4852 **D**:4848	Consecutive scans	5.77	6	t1.3
#2 **M**:5349 **D**:5352	20 scans apart	4.64	3	t1.4
#3 **M**:5349 **D**:5352	**R**(0)**T**(1)[#2]	4.64	38	t1.5
#4 **M**:4852 **D**:4848	**R**(10)**T**(3)[#1]	11.66	83	t1.6

The value of aerial imagery obtained via active range sensing for aiding ground vehicle navigation is being recognized within the UGV community. For example, in [34], aerial and ground views from unmanned vehicles are registered by extracting a geometrically consistent set of correspondences using surface signatures from which a registration transformation is estimated. It is not clear, given the computational burden associated with the extraction of surface signatures, whether this approach can be implemented in real-time. In [33], an aerial vehicle, a Flying Eye (FE), flies ahead of an UGV acting as a 'scout' to detect difficult obstacles from an overhead perspective thus benefitting ground vehicle navigation. The above article briefly mentions the need for registering the data from the FE to the ground vehicle but the details of the registration process are not presented. The hybrid approach proposed in this article exploits the simplicity and speed of the iterative closest point algorithm thus lending itself to real-time implementation.

The underlying assumption in the iterative registration algorithm is that the rotation angle between the range images that need to be registered is not too large and also that these images are not too far apart. For the current case of UAV and UGV LADAR data, this assumption is overly restrictive and an aiding mechanism for the registration of the range images becomes necessary.

The correspondence determination step is the most difficult and computationally expensive step of the iterative algorithm. Despite the apparent simplicity of this problem, establishing reliable correspondences is extremely difficult as the UGV is subjected to heavy pitching and rolling motion characteristic of travel over undulating terrain. This is further exacerbated by the uncertainty of the location of the sensor platform relative to the global frame of reference. In addition to these factors, noise inherently present in LADAR range images complicates the process of determining reliable correspondences. One solution to overcome the above deficiencies is to extract naturally occurring view-invariant features, for example, corners, from the LADAR scans. Such *control points* can then be used for establishing reliable registration with the ICP algorithm converging to the global minimum.

Towards guaranteeing robust and accurate registration, we first obtain the z translation value by estimating the ground z (elevation) values on the UGV and UAV LADAR data in the vicinity of the UGV's current location. For the UGV, the ground values are obtained from the LADAR points that are within a given radius immediately in front of the vehicle and those for the UAV are obtained by finding the minimum of the LADAR values. Then we project the UAV and UGV LADAR data into the base ground planes as depicted in Figure 5(a) and construct the feature planes by using the Canny edge detector [5]. The corner features are detected based on the intersections of lines formed by edges. The corner features are independently extracted from both LADAR data sets by considering those points that are above a given height from the ground as shown in Figure 5(b).
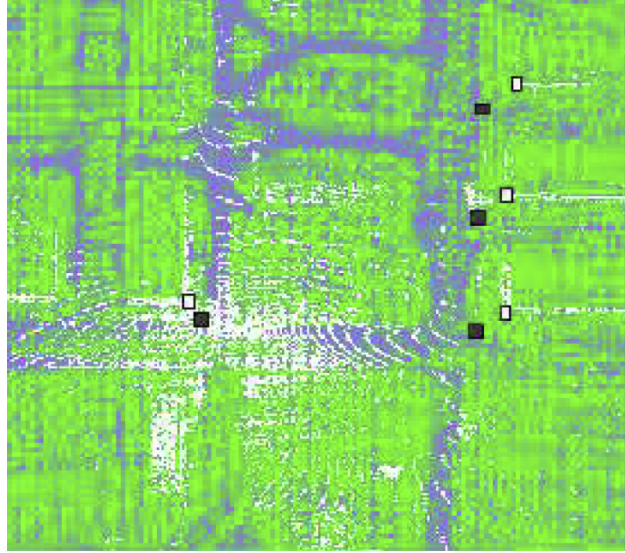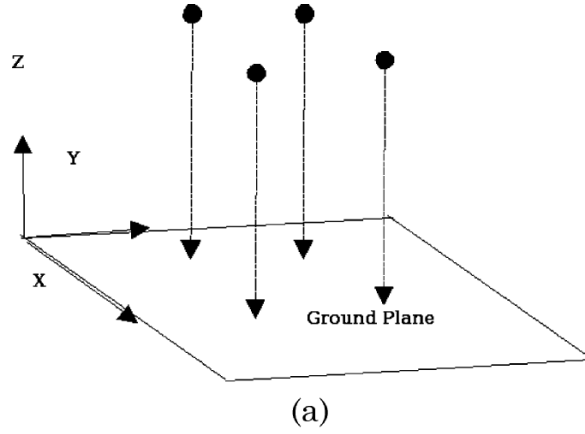
Figure 5. Projection of LADAR data to base ground planes is shown in (a). The extracted features (*corners*) from the UGV (*black*) and UAV (*white*) LADARs are shown in (b) as *white and black squares*, respectively.

The two sets of the projected corner points (UAV LADAR set: **A** and UGV LADAR set: **G**) are used to estimate a 2D translation. Given two sets of 2D corner points:

$$\mathbf{A} \triangleq \mathbf{a}_j = \begin{bmatrix} a_{1j} \\ a_{2j} \\ \vdots \\ a_{nj} \end{bmatrix}; \; j = 1, 2, \ldots n; \; \mathbf{G} \triangleq \mathbf{g}_k = \begin{bmatrix} g_{1k} \\ g_{2k} \\ \vdots \\ g_{nk} \end{bmatrix}; \; k = 1, 2, \ldots n;$$

To find a translation along the x and y directions, we first calculate the means of sets **A** and **G**: 377 378

$$\overline{\mathbf{a}} = \frac{1}{n} \sum_{j=1}^{n} \mathbf{a}_j; \quad \overline{\mathbf{g}} = \frac{1}{n} \sum_{k=1}^{n} \mathbf{g}_k;$$

The difference between the means of x, y and that between the aerial and ground z values provide a rough estimate of the required 3D translation between the two sets of LADAR data. The 3D translational offset when applied to the UGV range image enables the ICP algorithm to provide reliable registration results. 381 382 383 384 385

4.1. EXPERIMENTAL SETUP AND RESULTS 386

The UAV LADAR produces a 3D range image at up to 6,000 terrain pts/s within a 100 m scanning range. For additional details, see [24, 25]. It provides an aerial survey map with significant information about existing topology and structures. 387 388 389
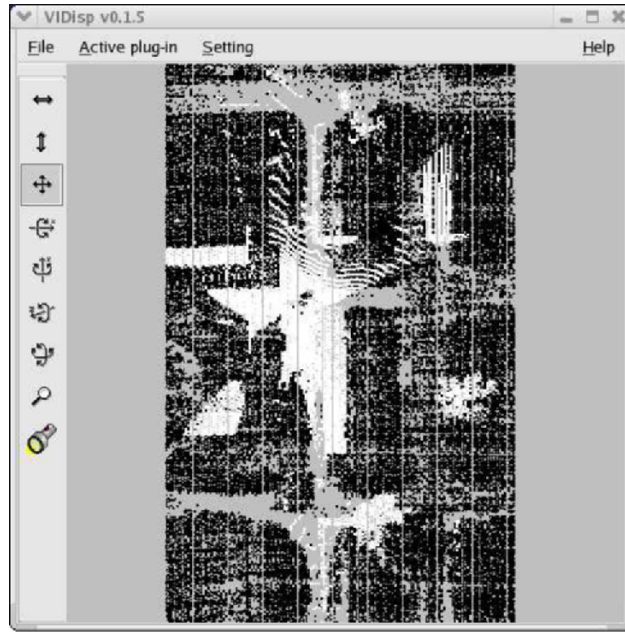
Figure 6 shows a top view of unregistered range images obtained from the UGV (in white) and UAV (in black) LADARs, respectively. Figures 7 and 8 depict the results of the feature-based registration algorithm. Figure 7(a) shows a top view of the LADAR range images after applying the translation obtained using the corner features. Figure 8(a) shows the results of the iterative registration algorithm applied to the LADAR range images in Figure 7(a). Figures 7(b) and 8(b) show a magnified view of stages depicted in Figures 7(a) and 8(a), respectively. From Figures 6–8, it is evident that the LADAR range images are registered. More results are available from [7]. 390 391 392 393 394 395 396 397 398

A similar sequence of results presented in Figures 9 and 10 again shows the efficacy of the proposed feature-based iterative algorithm in registering aerial and ground LADAR range images. 399 400 401
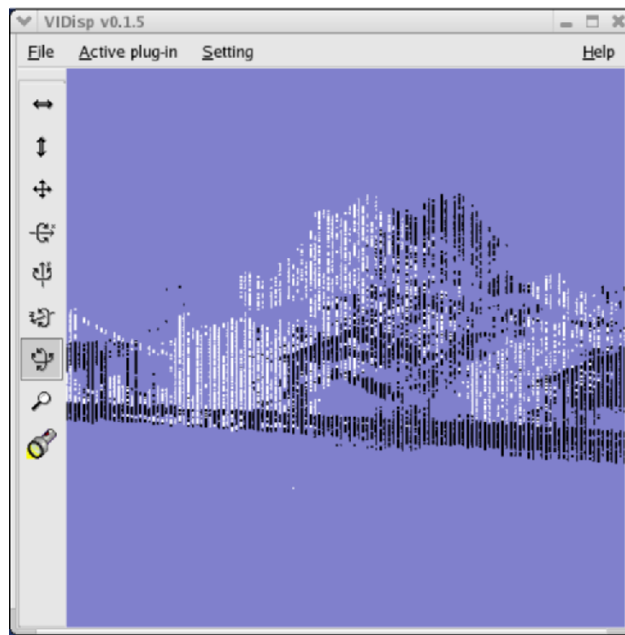
5. Conclusions and Further Work 402

Registering 3D range images from unmanned ground and aerial vehicles was the main theme of this article. The need for such registration is motivated by the requirement to continually estimate the position of the unmanned vehicle within accuracy bounds dictated by a particular mission even when the GPS position estimates are unreliable or unavailable. By making suitable modifications to the ICP algorithm it was shown that the modified algorithm provides reliable and robust registration in rugged terrain and urban environments for registering successive range images obtained from two different LADARs on a UGV. 403 404 405 406 407 408 409 410

The proposed algorithm was then extended to register aerial images obtained from a UAV with those from the UGV. A hybrid approach was proposed to this end by combining the modified ICP algorithm with a feature-based method. The 411 412 413
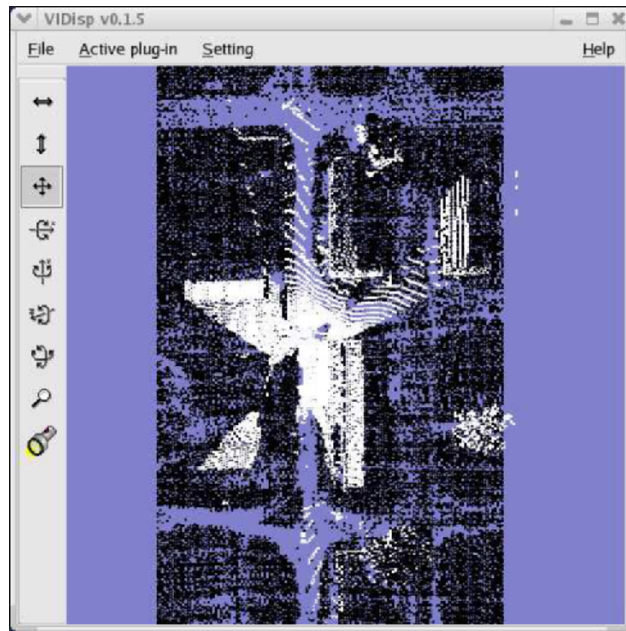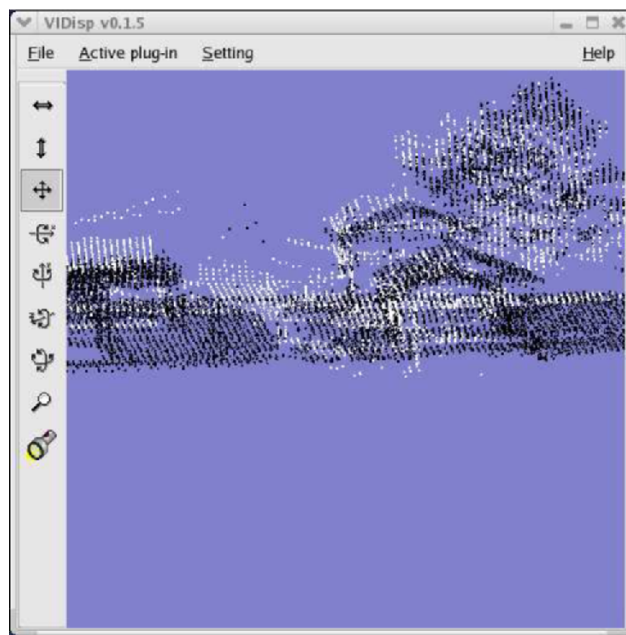
R. MADHAVAN ET AL.

(a)

(b)

Figure 6. A top view of unregistered UGV (*black*) and UAV (*white*) LADAR range images is shown in (a). A magnified side view of (a) is shown in (b).

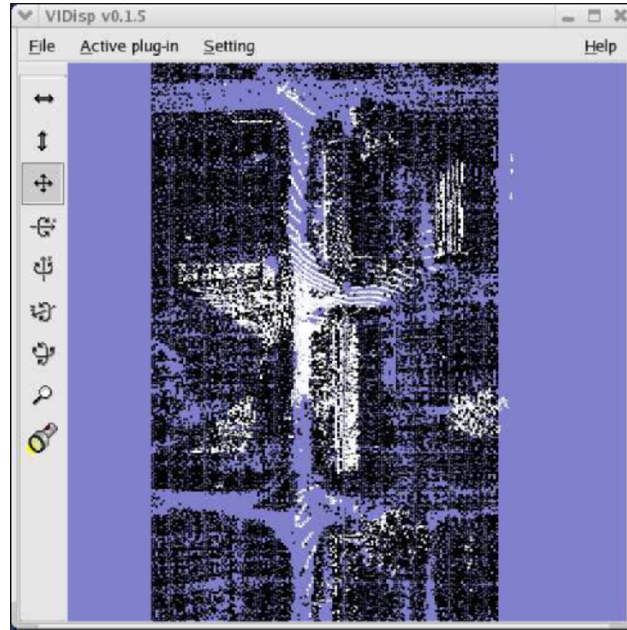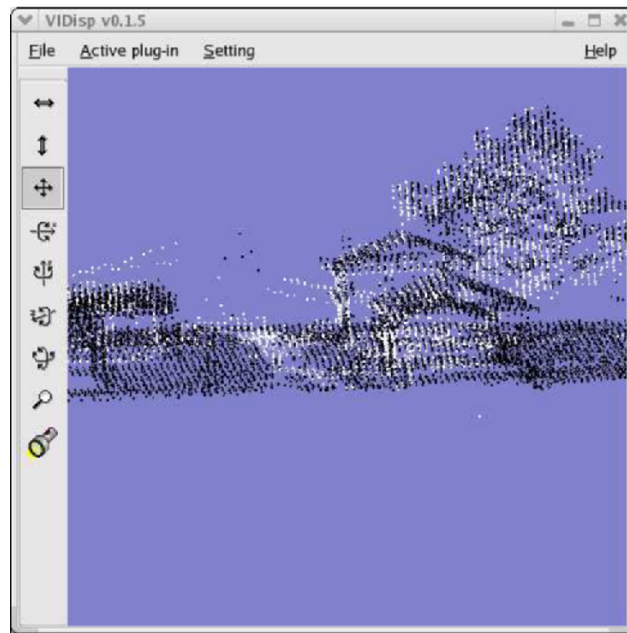TEMPORAL RANGE REGISTRATION FOR UNMANNED GROUND AND AERIAL VEHICLES

(a)

(b)

Figure 7. A top view of the feature-based translation obtained using the extracted corners is shown in (a) and a magnified side view of the same is shown in (b).

(a)

(b)

Figure 8. (a) shows a top view of the registered UAV (*black*) and UGV (*white*) LADAR range images obtained by utilizing the feature-based translation results and (b) is a magnified view of (a). See text for further details.
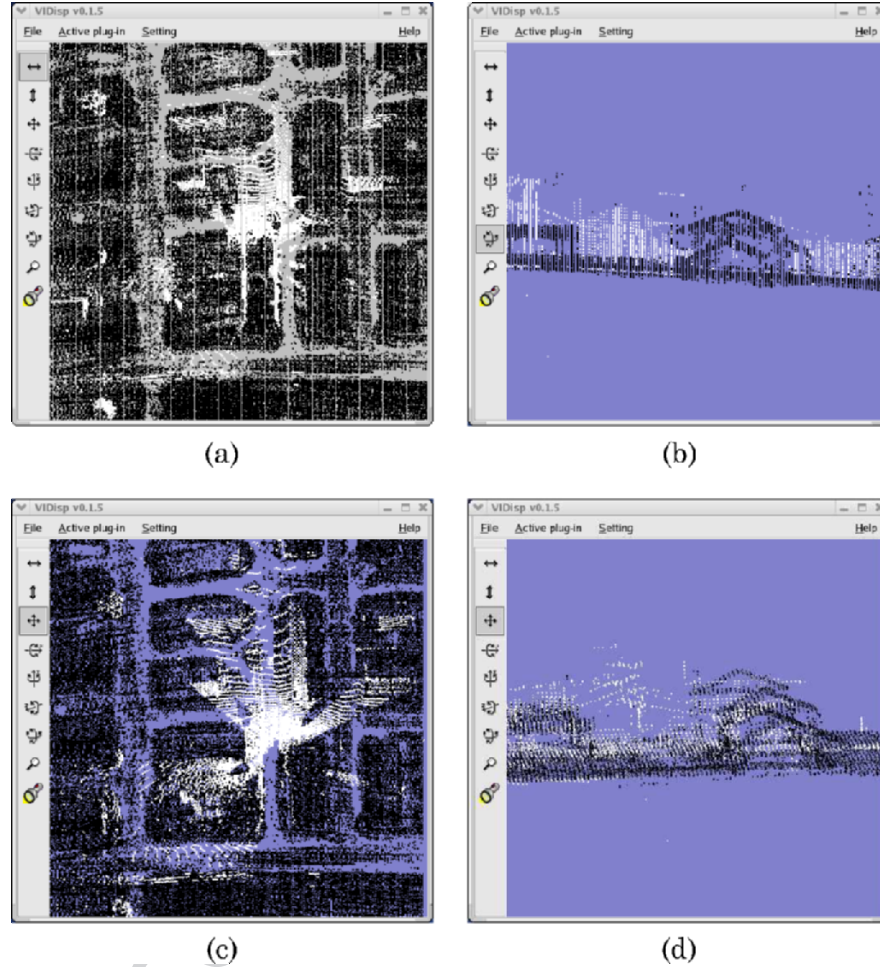
Figure 9. A top view of unregistered range images of UGV (*black*) and UAV (*white*) LADARs and the feature-based translation obtained using the extracted corners are shown in (a) and (c), respectively. (b) and (d), respectively, show magnified side views of their counterparts in the *left column*.

feature-based hybrid approach was also shown to be effective in producing reliable registration for UGV navigation.

The results presented in the article demonstrated the potential of this approach lending itself to real-time implementation. For practical purposes, the sets of LADAR data utilized in this article can be assumed to be of the same resolution even though typically the aerial data tend to be of lower resolution than that of the UGV LADAR. To address this issue, we are currently developing schemes for use within the ICP algorithm that will inherently account for varying resolution in data sets that need to be registered. Towards this, we are also de-
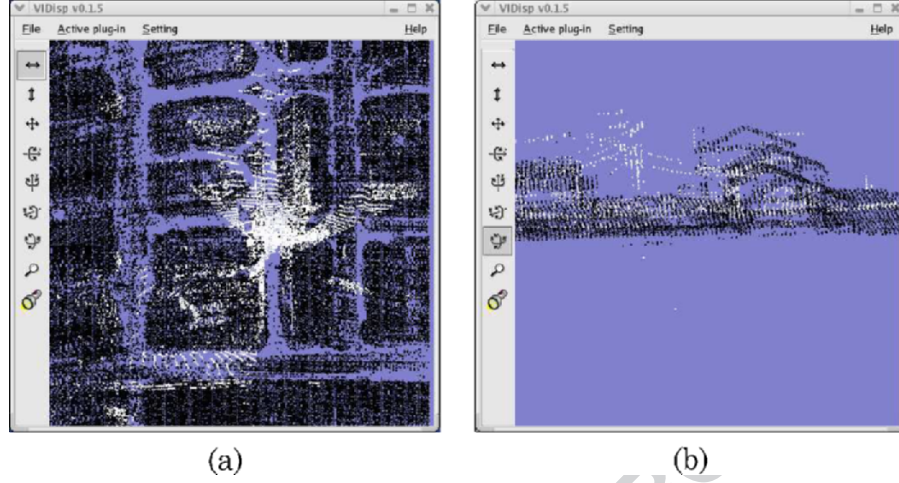
R. MADHAVAN ET AL.

Figure 10. The registered UAV (*black*) and UGV (*white*) LADAR range images obtained by utilizing the feature-based translation results are shown in (a). (b) shows a magnified side view of (a).

veloping corner detection schemes using the Harris [11] and SUSAN corner   431
detectors [32] on the 3D projected base ground planes.   432

As ICP will only converge to the closest local minimum, in this article, the   433
use of control points enabled us to guarantee that this local minimum will cor-   434
respond to the actual global minimum. If wrong convergence proves to be an   435
issue in cases where control points cannot be established, stochastic optimization   436
algorithms (e.g., Simulated Annealing) can be used to alleviate this problem. SA   437
is extremely slow in converging to the global minimum and thus a hybrid al-   438
gorithm that combines it with the proposed iterative algorithm would be more   439
appropriate. As the convergence of the algorithm depends on an initial estimate,   440
a sufficiently good initial estimate is required for superior registration. An initial   441
estimate is almost always available in our case as it can be obtained from either   442
the vehicle's dead reckoning or GPS estimates.   443

Computing the correspondence is the most computationally expensive part of   444
the algorithm. *kd-trees* have been proposed for faster correspondence where the   445
complexity is reduced from $O(N_\mathbf{D}N_\mathbf{M}) \rightarrow O(N_\mathbf{D}logN_\mathbf{M})$. We have also employed   446
Quaternions [17] (instead of SVD) to determine the 3D transformation but it   447
results only in a slight improvement in the resultant registration for the tested   448
field data.   449

In case of non-unique data sets (meaning less 'structure' in the environment),   450
extraction of naturally occurring control points was shown to be a good means of   451
guaranteeing the convergence of the algorithm for reliable registration. In the   452
field trials, the vehicle was driven at a top speed of 20 mph for which case a good   453
initial estimate is readily available and this immensely speeds up the corre-   454

spondence determination. In the results reported in this article, we have been able   455
to establish reliable registration in 10–12 iterations (at the most). This makes the   456
proposed registration scheme very viable for real-time implementation.   457

We have evaluated the performance of the registration algorithm for UGV   458
navigation and have developed measures to quantify the performance of the   459
algorithm [23]. The quality of the 3D registration will significantly improve if the   460
uncertainty of the LADAR range images are taken into account and has been so   461
verified for 2D laser scan registration [21]. We are currently investigating the   462
extension of these results to the 3D case. To quantify the accuracy of the reg-   463
istration results, we are investigating methods for estimating a covariance matrix   464
of the error function that is minimized. We anticipate the covariance matrix to be   465
useful when fusing the position estimates obtained via registration with other   466
sensors.   467

We have not had an opportunity to subject our LADAR to factors that might   468
cause performance deterioration (for e.g., rain and fog). But these effects have   469
been studied (on another LADAR) at NIST [16] in which the authors discuss   470
the back scattering effect caused by fog that causes a spurious range value to   471
be returned by the LADAR. There also exist research in the open literature   472
on performance degradation of 2D LADAR under rainy conditions. For the   473
LADAR used in the research reported in this article, these effects remain to be   474
investigated.   475

References   476

1. Albus, J. et al.: *4D/RCS Version 2.0: A Reference Model Architecture for Unmanned Vehicle*   477
   Systems. Technical Report NISTIR 6910, National Institute of Standards and Technology,   478
   Gaitherburg, MD 20899, USA, 2002.   479
2. Albus, J.: Outline for a theory of intelligence, *IEEE Trans. Syst. Man Cybern.* **21**(3) (1991),   480
   473–509.   481
3. Arun, K., Huang, T., and Blostein, S.: Least-squares fitting of two 3-D point sets, *IEEE*   482
   Trans. Pattern Anal. Mach. Intell. **9**(5) (1987), 698–700.   483
4. Besl, P. and McKay, N.: A method for registration of 3-D shapes, *IEEE Trans. Pattern Anal.*   484
   Mach. Intell. **14**(2) (1992), 239–256.   485
5. Canny, J. F.: A computational approach to edge detection, *IEEE Trans. Pattern Anal. Mach.*   486
   Intell. **8**(6) (November 1986), 679–698.   487
6. Cox, I.: BLANCHE – An experiment in guidance and navigation of an autonomous robot   488
   vehicle, *IEEE Trans. Robot. Autom.* **7**(2) (1991), 193–204.   489
7. Downs, A., Madhavan, R., and Hong, T.: Registration of range data from unmanned aerial   490
   and ground vehicles, in: *Proc. of the Applied Imagery Pattern Recognition Workshop*,   491
   October 2003, pp. 45–50.   492
8. Drumheller, M.: Mobile robot localization using sonar, *IEEE Trans. Pattern Anal. Mach.*   493
   Intell. **9**(2) (March 1987), 325–332.   494
9. Forsberg, J., Larsson, U., and Wernersson, A.: Mobile robot navigation using the range   495
   weighted hough transform, *IEEE Robot. Autom. Mag. – Special Issue on Mobile Robots*   496
   21 (March 1995), 18–26.   497

10. Grimson, W. and Lozano-Perez, T.: Localizing overlapping parts by searching the interpretation tree, *IEEE Trans. Pattern Anal. Mach. Intell.* **9**(4) (July 1987), 469–482.

11. Harris, C. and Stephens, M.: A combined corner and edge detector, in: *Proc. of the Fourth Alvey Vision Conference*, September 1988, pp. 147–151.

12. Hebert, M., Caillas, C., Krotkov, E., Kweon, I., and Kanade, T.: Terrain mapping for a roving planetary explorer, in: *Proc. of the IEEE International Conference on Robotics and Automation*, 1989, pp. 997–1002.

13. Hebert, M., Kanade, T., and Kweon, I.: 3-D Vision techniques for autonomous vehicles, in: *Proc. of the NSF Range Image Understanding Workshop*, 1988, pp. 273–337.

14. Hoffman, B., Baumgartner, E., Huntsberger, T., and Schenker, P.: Improved rover state estimation in challenging terrain, *Auton. Robots* **6**(2) (April 1999), 113–130.

15. Hong, T., Balakirsky, S., Messina, E., Chang, T., and Shneier, M.: A hierarchical world model for an autonomous scout vehicle, in: *Proc. of the SPIE International Symposium on Aerospace/Defense Sensing, Simulation, and Controls*, April 2002, pp. 343–354.

16. Hong, T., Legowik, S., and Nashman, M.: Obstacle detection and mapping system, Technical Report NISTIR 6213, National Institute of Standards and Technology, Gaithersburg, MD 20899, USA, August 1998.

17. Horn, B. K. P.: Closed form solution of absolute orientation using unit quaternions, *J. Opt. Soc. Am.* **4**(4) (April 1987), 629–642.

18. Kweon, I. and Kanade, T.: High resolution terrain map from multiple sensor data, in: *Proc. of the IEEE International Workshop on Intelligent Robots and Systems*, 1990, pp. 127–134.

19. Larsson, U., Forsberg, J., and Wernersson, A.: On robot navigation using identical landmarks: integrating measurements from a time-of-flight laser, in: *Proc. of the IEEE Conference on Multisensor Fusion and Integration for Intelligent Systems*, October 1994, pp. 17–26.

20. Lu, F.: *Shape Registration Using Optimization for Mobile Robot Navigation*. PhD thesis, Dept. of Computer Science, University of Toronto, 1995.

21. Madhavan, R. and Durrant-Whyte, H.: Terrain aided localization of autonomous ground vehicles, *Special Issue of the J. Autom. Constr. (Invited)* **13**(1) (January 2004), 69–86.

22. Madhavan, R., Hong, T., and Messina, E.: Temporal range registration for unmanned ground and aerial vehicles, in: *Proc. of the IEEE International Conference on Robotics and Automation*, April 2004, pp. 3180–3187.

23. Madhavan, R. and Messina, E.: Performance evaluation of temporal range registration for unmanned vehicle navigation, *Integrated Computer-Aided Engineering; Special Issue on Performance Metrics for Intelligent Systems (Invited)* **12**(3) (2005), 291–303.

24. Miller, R., Amidi, O., and Delouis, M.: Arctic test flights of the CMU autonomous helicopter, in: *Proc. of the Association for Unmanned Vehicle Systems International 26th Annual Symposium*, 1999.

25. Miller, R. and Amidi, O.: 3-D Site mapping with the CMU autonomous helicopter, in: *Proc. of the 5th International Conference on Intelligent Autonomous Systems*, June 1998.

26. Olson, C.: Mobile robot self-localization by iconic matching of range maps, in: *Proc. of the 8th International Conference on Advanced Robotics*, May 1997, pp. 447–452.

27. Olson, C.: Probabilistic self-localization for mobile robots, *IEEE Trans. Robot. Autom.* **16**(1) (2000 February), 55–66.

28. Schiele, B. and Crowley, J.: A comparison of position estimation techniques using occupancy grids, in: *Proc. of the IEEE International Conference on Robotics and Automation*, May 1994, pp. 1628–1634.

29. Shaffer, G.: Two-dimensional mapping of expansive unknown Areas, PhD thesis, Carnegie Mellon University, 1992.

30. Shneier, M., Chang, T., Hong, T., Cheok, G., Scott, H., Legowik, S., and Lytle, A.: A repository of sensor data for autonomous driving research, in: *Proc. of the SPIE Unmanned Ground Vehicle Technology V*, April 2003.

31. Shoemaker, C. and Bornstein, J.: The demo III UGV program: A testbed for autonomous navigation research, in: *Proc. of the IEEE ISIC/CIRA/ISAS Joint Conference*, September 1998, pp. 644–651.

32. Smith, S. M. and Brady, J. M.: SUSAN – a new approach to low level image processing, *Int. J. Comp. Vis.* (1997 May), 45–78.

33. Stentz, A. et al.: Real-time, multi-perspective perception for unmanned ground vehicles, in: *Proc. of the AUVSI Unmanned Systems Conference*, July 2003.

34. Vandapel, N., Donamukkala, R., and Hebert, M.: Experimental results in using aerial LADAR data for mobile robot navigation, in: *Proc. of the International Conference on Field and Service Robotics*, July 2003.

35. Weiß, G., Wetzler, C., and von Puttkamer, E.: Keeping track of position and orientation of moving indoor systems by correlation of range-finder scans, in: *Proc. of the IEEE/RSJ International Conference on Intelligent Robots and Systems*, September 1994, pp. 595–601.

36. Zhang, Z.: Iterative point matching for registration of free-form curves and surfaces, *Int. J. Comput. Vis.* **13**(2) (1994), 119–152.

AUTHOR QUERY

AUTHOR PLEASE ANSWER QUERY.

No Query.